

# Liver Vessels Segmentation Using a Hybrid Geometrical Moments/Graph Cuts Method

Simon Esneault, Cyril Lafon, *Member, IEEE*, and Jean-Louis Dillenseger\*

**Abstract**—This paper describes a fast and fully automatic method for liver vessel segmentation on computerized tomography scan preoperative images. The basis of this method is the introduction of a 3-D geometrical moment-based detector of cylindrical shapes within the minimum-cut/maximum-flow energy minimization framework. This method represents an original way to introduce a data term as a constraint into the widely used Boykov's graph cuts algorithm, and hence, to automate the segmentation. The method is evaluated and compared with others on a synthetic dataset. Finally, the relevancy of our method regarding the planning of a necessarily accurate percutaneous high-intensity focused ultrasound surgical operation is demonstrated with some examples.

**Index Terms**—Geometrical moments, graph cuts, hepatocellular carcinoma (HCC), liver segmentation, vessels extraction.

## I. INTRODUCTION AND STATE OF THE ART

**H**EPATOCELLULAR carcinoma (HCC) is the third most common cause of mortality from cancer, with incidences rising in western countries [1]. At an early stage, HCC is commonly confined to a solitary mass, which is potentially curable by a percutaneous surgical resection, such as percutaneous ethanol injection, or radiofrequency ablation [2]. Radiofrequency treatment is one of the most widely used HCC therapies. The main drawback of radiofrequency treatment is that the heating process is locally disturbed by the presence of nearby blood vessel acting as coolers, resulting in a partial therapy.

In addition to the hyperthermic interstitial techniques, ultrasound surgery is being proposed within this interstitial applicators context at an experimental stage [3], [4]. The therapeutic ultrasound device is composed of a small (3 mm × 10 mm) planar ultrasonic transducer encapsulated in a  $\varnothing$  4-mm-cylindrical interstitial applicator. The surgical protocol is as follows: 1) the

applicator is set within or on the boundary of the hepatic tumor under ultrasound image guidance; 2) the therapy consists of a sequence of high-intensity ultrasound shots that can be controlled in intensity and duration. After each exposure, the applicator can be rotated by a specific angle in order to heat the tissues according to the tumor geometry. The advantages to this ultrasound technique include more precise control in depth and direction than other interstitial heating modalities, and perhaps, more adaptability to the specific treatment, i.e., for compensating the blood vessels cooling influence.

Like any other minimally invasive image-guided therapy, clinical application requires the definition of a precise planning at the preoperative stage as well as during the intervention itself, including the tracking and the controlling of the therapeutics effects. Thus, the anatomical description of the tumor-neighboring hepatic vessels is of crucial importance for therapeutic planning for two different reasons: 1) to determine the best path for the interstitial applicator and 2) to provide the information for an accurate dosimetry simulation that takes the blood vessels presence into account.

The segmentation of the detailed hepatic volume, with all its anatomical components, is still an open question [5]. In previous work, we proposed graph-cuts-based technique that enabled the segmentation of the liver and tumor [6]. However, this method gave poor results when used to solve the vessel segmentation problem. The poor results are mostly due to the shrinking bias problem that also occurs when working with level-set or snakes. For local thin and elongated structures, the summed cost of the cuts along the natural boundary will be higher than the one across the structures, leading to an incorrect segmentation. The natural response to avoid this bias is to locally constrain the graph with higher cost value along thin boundaries.

Several specific methods have been proposed to segment vessels in a computed tomography (CT) volume [7]. These methods, adapted from generic segmentation algorithms, mainly rely on intensities analysis, generalized cylinders approximations, multiscale or skeletization schemes, or deformable model approaches. Selle *et al.* [8], for example, define an optimal intensity threshold using region growing, but their method appears to be only suitable for large vessels. Level-sets methods [9] have also proved to be suitable for magnetic resonance angiography (MRA)-segmentation, but require good initialization and typically use speed functions that implicitly assume good contrast data. These two methods are typical examples of generic segmentation algorithms adapted to the vessel extraction. But, usually such methods faced the complexity of the vascular trees and their images (thin elongated structures, low contrast, inhomogeneous structures, high number of bifurcations, noise induced by the imaging of the microvascularization, etc.).

Manuscript received January 30, 2009; revised July 3, 2009. First published September 25, 2009; current version published January 20, 2010. This work was supported in part by the National Select University Technologies, Inc., project under Agence Nationale de la Recherche Grant ANR05RNTS01106. Asterisk indicates corresponding author.

S. Esneault is with the Institut National de la Santé et de la Recherche Médicale (INSERM) U642, F-35000 Rennes, France, and also with the Laboratoire Traitement du Signal et de l'Image (LTSI), Université de Rennes 1, F-35000 Rennes, France (e-mail: simon.esneault@univ-rennes1.fr).

C. Lafon is with the Institut National de la Santé et de la Recherche Médicale (INSERM) U556, Lyon, France, and also with the Université Claude Bernard Lyon 1, Lyon, F-69003 France (e-mail: cyril.lafon@inserm.fr).

\*J.-L. Dillenseger is with the Institut National de la Santé et de la Recherche Médicale (INSERM) U642, F-35000 Rennes, France, and also with the Laboratoire Traitement du Signal et de l'Image (LTSI), Université de Rennes 1, F-35000 Rennes, France (e-mail: jean-louis.dillenseger@univ-rennes1.fr).

Color versions of one or more of the figures in this paper are available online at <http://ieeexplore.ieee.org>.

Digital Object Identifier 10.1109/TBME.2009.2032161

An other approach is to take the vascularization tree-like topology into account by tracking the vessel. In this class of method, starting from a focus known to be a vessel, the centerlines of the vascular tree are iteratively tracked using local features, such as Hessian [10] or geometrical moments [11]. For example, some previous work based on the vessel local characterization by geometrical moments, belongs to this category and has shown some good abilities on MRA [11], and CT scan for lower limbs vessels extraction [12]. In both cases, the algorithm follows the same iterative scheme: from interactively selected seed points, the local radius, orientation, and center of the vessel are estimated with an iterative process using 3-D geometric moment. After local convergence, the process is then repeated in the direction of the previously detected orientation, and hence, tracking the vessel local features. This method is fast and robust, but requires special routines to handle branch points and some user-interaction to initialize. The authors also reported that in case of high curvature or complex bifurcation, the tracking can be stopped. These kinds of drawbacks seems to be, generally, shared by the other tracking approaches. Therefore, such a class of methods is not suitable in our segmentation scheme, as the liver vessel tree presents a high vascularization with a lot of bifurcations. We propose to take advantage of both approaches in a quick, accurate, and fully automatic method for the hepatic vessel segmentation. Initially, it is first based on an automatic tubular structure detection using geometrical moments. The detected structures are described as vessel presence probabilities and set as constraints in the graph cuts segmentation. The outline of this paper is as follows. Section II will present the method and describe our approach to insert data-related information into a graph cuts segmentation. Some results are presented in Section III, and a conclusion is given in Section IV.

## II. HYBRID METHOD FOR VESSEL EXTRACTION: GENERAL SCHEME

The proposed approach is principally based on two classes of methods: a 3-D geometrical moment-based detector to localize the center of the vessel, its diameter, and local direction. This model is then used as a local constraint into a graph cuts algorithm, which delivers the final segmentation.

### A. 3-D Geometrical Moment Tubular Structures Detection Process

The method relies on the local modeling of the vessels using geometrical moments [11]. Near a specific voxel, a vessel is locally modeled as a cylinder described by the following parameters (see Fig. 1): its orientation ( $\alpha, \beta$ ), position  $P$  at a subvoxel accuracy, and radius  $R$ . With the assumption of an *a priori* knowledge of the mean intensities of the vessel and the background, the model's parameters can be analytically identified from the gray level geometrical moments computed in a spherical window centered on the voxel. The moment-based local model estimation has proved to be robust compared to other methods, because of its integrative computation nature [13].

Classically, this model is used in a vessel spatial tracking scheme from interactively selected seeds points [11], [12]. In

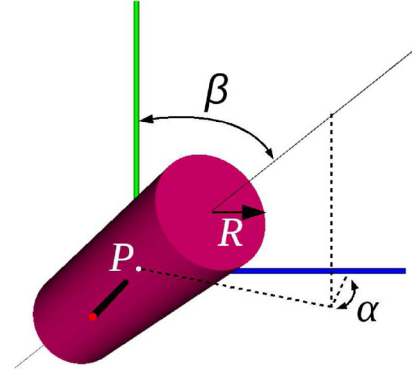


Fig. 1. Local vessel model, with  $\alpha, \beta$  the orientation angles,  $P$  the center position, and  $R$  the radius.

our specific case, the hepatic vascularization is characterized by a high number of bifurcations that can not be handled directly by the tracking process.

Complex geometrical tracking algorithm is not necessary for this method; therefore, we propose to use this model in a slightly different manner: 1) the local cylinder detector is applied on the voxels of the whole volume in an exhaustive way; 2) the voxels (and their associated local model) that present the highest probability to be in a vessel are selected; and 3) the results of this research is a set of local models of the vessels not necessarily connected to one another. This information is then used in the graph cuts process in order to achieve the global vessels segmentation.

The following is a detailed scheme of this detection.

**Initialization:** Given that the focus is to design a segmentation framework fast enough to be used in a clinical routine, we first define a research subarea in order to restrict the amount of voxel candidates for detection. The idea is to roughly select all voxels of the volume, which potentially could be in a vessel. For this, we apply thresholding, rated median filter, and 3-D skeletonization to the volume. The different filters parameters are chosen to achieve a selection with a high sensitivity (nearly all of the vessels voxels are correctly classified) and a small specificity (not all of the background voxels are correctly classified). Hence, a map  $A^*$  of candidate voxels  $P_i$  remains.

**Local modeling and detection:** A multiscale tubular-structure-detection method is applied for each candidate point  $P_i$  of  $A^*$ . It follows an iterative scheme [12] as follows.

- 1) *Position refinement:* An iterative process moves until convergence, the center of the local spherical window toward the center of gravity with a subvoxel precision using the geometrical moments of order 1.
- 2) *Cylinder parameters estimation:* The orientation and the radius of the estimated cylinder in the 3-D space are computed from analytical expressions, developed in [11], using the 3-D geometrical moments up to order 2.
- 3) *Resolution refinement:* The local spherical window size is adapted according to the estimated vessel radius.

- 4) *Decision*: If the local spherical window converges within a specific margin, the estimated cylinder is retained and appended to a candidate list.

The result of this detection step is a list of cylinder parameters in the 3-D space. None of these cylinders are explicitly connected to each other; they give information about the likelihood of the presence of a vessel. These parameters will be used as local shape information for the graph cuts' global optimization.

### B. Graph Cuts Global Optimization and Segmentation

A number of problems in computer vision can be expressed as energy minimization. Within this class of methodologies, Greig *et al.* [14] and then Boykov *et al.* [15] proposed an energy minimization method based on the partitioning of a graph into two subgraphs by a minimum-cut/maximum-flow algorithm (min-cut/max-flow graph cuts).

This graph partitioning algorithm is perfectly adapted to a volume binary classification issue [16], [17]. Moreover, the transcription of a segmentation issue into an energy minimization framework makes it possible to encode various characteristics of the data: classification training, degree of similarity between voxels of the same class (region-based approaches), changes between classes (boundary-based approaches), etc. As it was demonstrated in [15], the total energy minimization for the volume segmentation follows a Gibbs model with a data term and a smoothing term. Therefore, the method is considered to be globally optimal with respect to an objective function for segmentation.

The segmentation problematic is described by a directional flow graph [16], [17]. The nodes set is defined by two particular nodes "source" S and "sink" T called terminal nodes and representing in our case, the class "vessel" and the class "background", respectively. The other nodes are intermediate nodes that correspond to the voxels of the 3-D volume. Directed weighted links connect the nodes. The link topology and the initial costs assigned to these links are derived from the energy function to minimize. Two kinds of links must be identified, which are as follows.

- 1) The *t-links* connecting voxel to the terminals S and T. "*t*" stands for terminal. The initial costs are derived from the data term and serve as segmentation hard constraints.
- 2) The *n-links* between a pair of intermediate nodes (voxel). The initial costs will code the dissimilarity between the two voxels. "*n*" stands for neighbors, meaning that the two nodes are usually close to each other, with an 8- or 26-neighborhood connectivity.

As initially introduced in Boykov's papers, the energy function used for segmentation is as follows:

$$E_T = E_{\text{region}} + E_{\text{boundary}} \quad (1)$$

where a data term  $E_{\text{region}}$  is an energy coding the probability that a voxel belong to the class "object" or "background" set on the *t-links* and a smoothing term  $E_{\text{boundary}}$  is an energy coding the local discontinuity between a pair of voxels represented by the *n-links*.

TABLE 1  
INITIAL WEIGHTS FOR GRAPH CUTS SEGMENTATION

arcs	costs	condition
$\{p, q\}$	$\lambda_2 \cdot \left\{ \frac{\exp(-(I_p - I_q)^2 / 2\sigma^2)}{\text{dist}(p, q)} \right\}$	for $\{p, q\} \in N$
$\{p, S\}$	$\lambda_1 \cdot P_{\text{region}}(p) + \lambda_3 \cdot C_{\text{vessel}}(p)$	for $p \in N$
	$\infty$	for $p$ a cylinder center
$\{p, T\}$	$\lambda_1 \cdot (1 - P_{\text{region}}(p))$	$p \in N$

Once the graph is build with the correct weight assigned to each links according to some relevant cost functions, a min-cut/max-flow combinatorial optimization algorithm [18], [19] is applied to the graph.

In the original version of the graph cuts algorithm, the regional term cost function is defined after an interactive process. The user interactively selects one or more points representing the object, and other points representing the background. Histograms are built from this labeling and probability density functions are extracted for each class and encoded in the graph.

In our method, instead of using these interactive labeling processes, we propose the previously extracted information as part of the segmentation cost function in two ways: first as automatic assignment of the regional term  $E_{\text{region}}$ , and also as a new data term energy  $E_{\text{vessel}}$  to constrain the graph cuts optimization to extract the vessels. The new energy equation is now as follows:

$$E_T = \lambda_1 E_{\text{region}} + \lambda_2 E_{\text{boundary}} + \lambda_3 E_{\text{vessel}} \quad (2)$$

with  $\lambda_{1,2,3}$  weights that control the balance between the energy terms.

The energy function described in (2) is encoded in a graph. The following is an explanation of how we translate each of these three terms as weighted arcs in the graph.

The initial costs associated to the  $E_{\text{boundary}}$  smoothing term are built, as suggested by Boykov *et al.* using an *ad hoc* function that penalizes discontinuities between adjacent voxels (see Table I).

The initial costs related to the data term  $E_{\text{region}}$  reflect the probability that a specific voxel belongs to, respectively, the vessel and background classes. We used the position  $P$  of each detected cylinders to automatically label some voxels as "vessel." The histogram built from the values on these points is used after normalization to define the probability density function  $P_{\text{region}}$ . The initial costs related to the data term  $E_{\text{vessel}}$  reflect the probability of a vessel presence. This information is given by the cylinders estimated in the detection process. The idea is to diffuse the strong information given by the cylinder to its neighborhood. The diffusion is promoted along the vessel axis and constrained perpendicularly to the axis, according to the vessel radius (see Appendix). Using this function, we create a local 3-D costs map for each cylinder. The final costs map  $C_{\text{vessel}}$  is the result of the combination of all the individual maps in order to take overlapping information into account.

Let  $N$  be the set of voxels or volume,  $\{p, q\}$  a set of neighbor nodes, the initial weights of the individual graph links are assigned to the graph, according to Table I.



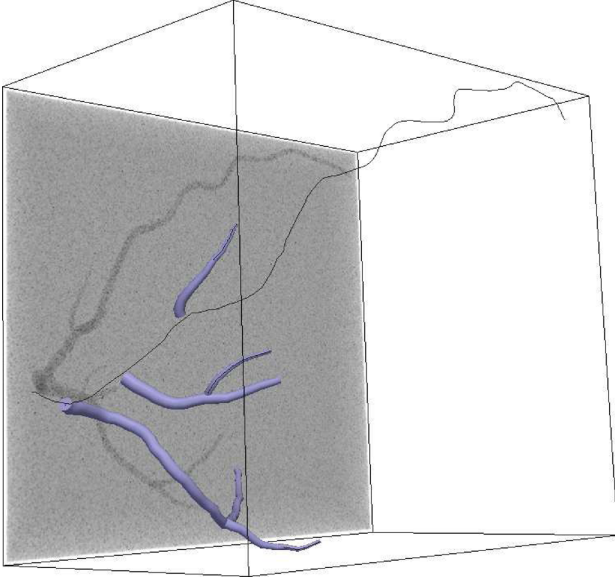


Fig. 2. Step of the phantom construction: centerlines, vessel mesh, and an MIP of the final volume. The parameter set of this phantom is:  $\{r = \{2, 6\}\text{mm}, v = 130, b = 100, \sigma_{\text{noise}} = 15\}$ .

Once the graph is built, min-cut/max-flow graph cuts algorithm is performed in order to extract the vessels.

### III. RESULTS AND DISCUSSION

#### A. Quantitative Evaluation

In order to validate our method, we create a 3-D digital vessels phantom. For geometry simplicity, our phantom is based on a real coronary artery tree description. The model is constructed from six extracted centerlines [20] and *ad hoc* chosen vessel diameters set, hence creating a realistic mesh.

A rasterization algorithm enables us to get a binary volume with the following characteristics: size of  $303 \times 413 \times 448$  voxels and spacing of  $0.7 \text{ mm} \times 0.7 \text{ mm} \times 0.7 \text{ mm}$ . The microvascularization is modeled by additive white Gaussian noise. The different parameters controlling the phantom are:  $r$  the vessel radius variation,  $b$  the background value,  $v$  the vessel value, and  $\sigma_{\text{noise}}$  the Gaussian noise standard deviation. Fig. 2 presents the several steps of the phantom construction: centerlines, vessels mesh, and a maximum intensity projection (MIP) of the final phantom volume with noise.

For the tests, a set of phantoms is created. The vessel geometry is fixed to  $r$ , decreasing from 6 (main branches) to 2 mm,  $v = 130$ , and  $b = 100$  with  $\sigma_{\text{noise}}$  varying from 0 to 50 with a step of 5.

We choose to compare our hybrid method with two others segmentation methods: a basic seeded region growing and the standard graph cuts algorithm. The specifications of each method are as follows.

- 1) The region growing is performed with 26-connectivity, with a single seed point interactively selected inside the vessel, and an aggregation criteria based on a voxel intensity threshold fixed at  $v - (\sigma_{\text{noise}}/2)$ .

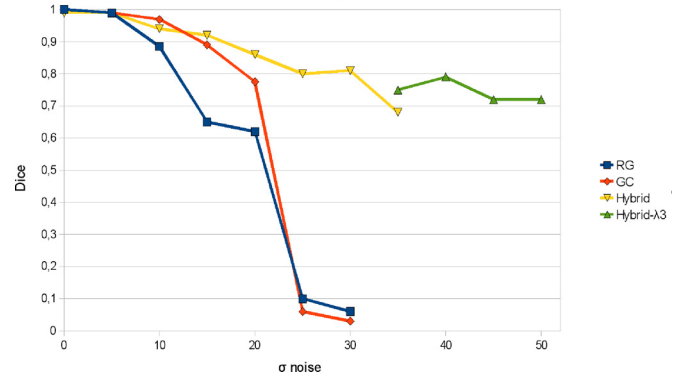


Fig. 3. Dice measure of the different methods versus  $\sigma_{\text{noise}}$ . Region growing (RG); classical graph cuts (GC); Hybrid method with balanced energies (Hybrid); Hybrid method with enhanced geometrical moment energy (Hybrid- $\lambda_3$ ).

- 2) The graph cuts algorithm is also performed with a 26-connectivity, the seed points are selected interactively and  $\lambda$  is set to 0.5.
- 3) The parameters of the hybrid method (see Table I) are set to:  $\lambda_1 = 0.5, \lambda_2 = 0.3, \lambda_3 = 0.2$ , and  $\sigma = 0.20$  with a 26-neighborhood connectivity.

For these two later methods, the graph was built using the Boykov–Kolmogorov’s C++ graph cuts implementation.<sup>1</sup>

The binary classification results of each of the three methods are compared to the initial model by two different ways: the mutual overlap approach and statistics on the signed distances between the borders of the model and estimated by the segmentation methods.

The mutual overlap approach, also known as the dice evaluation, is based on computing the area of overlap between ground truth and a segmented region

$$M_{\text{MO}} = \frac{2\text{MO}}{A_1 + A_2} \quad (3)$$

where  $A_1$  is the area of the segmented region,  $A_2$  is the area of the ground truth (the phantom), and MO is the area of their mutual overlap.

Fig. 3 represents the dice measure of the three methods for a parameter  $\sigma_{\text{noise}}$  varying from 0 to 30. It clearly shows the robustness of our method compared to the others. With small noise, all the three methods shows similar results. However, with higher  $\sigma_{\text{noise}}$ , region growing ( $\sigma_{\text{noise}}$  above 15) and the classical graph cuts ( $\sigma_{\text{noise}}$  above 25) failed to extract the vascular tree. For the region growing algorithm, the simplicity of the aggregation criteria is sufficient to explain its failure. The classical graph cuts seems more robust for reasonable noise. However, when the noise increase, the smallest branches are no more detected. Some more interaction by adding seed points could improve the result. But practically in extreme noisy conditions, even with more than 100 seeds points, the algorithm failed to detect all the branches and/or to connect them. So, our method seems to be the most robust in such conditions. In our opinion, this advantage is induced by the geometrical moment computation that is robust

<sup>1</sup><http://www.cs.ucl.ac.uk/staff/V.Kolmogorov/software.html>.

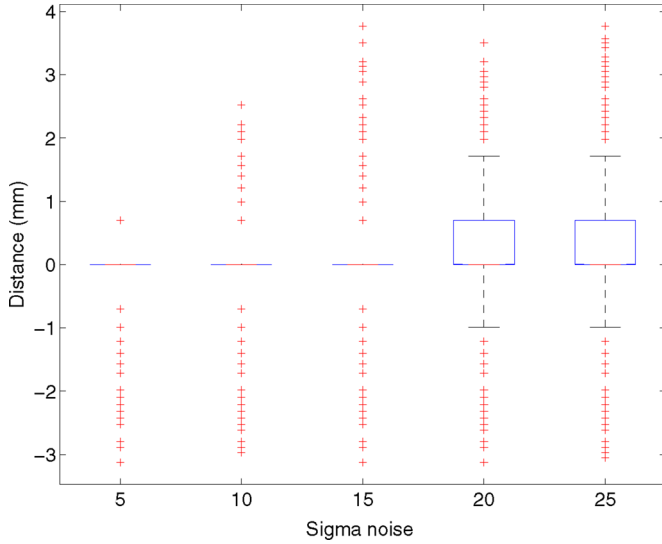


Fig. 4. Distance to the border boxplots for the hybrid method with  $\sigma_{\text{noise}}$  varying from 5 to 25.

to noise because of its integrative form. Moreover, the advantage to add a robust geometrical constraint to the standard graph cuts is highlighted in this test.

With  $\sigma_{\text{noise}}$  above 30, our method also misses the smallest vessels. However, by enhancing the weight of the geometrical moment energy (e.g.,  $\lambda_1 = 0.3$ ,  $\lambda_2 = 0.1$ , and  $\lambda_3 = 0.6$ ), our method is still able to detect the vessels (see Fig. 3, label: hybrid- $\lambda_3$ ), but with an overestimation of the vessel radius. This can be explained by the fact that the noise near the vessel border is detected by our multiscale estimator as small cylinders. With a high  $\lambda_3$ , these small cylinders are included in the graph cuts scheme as high constraints, leading to locally overestimated vessel radii.

On the second evaluation, we perform some statistical measurements on the signed Euclidian distances between each surface point of the model vessels border to the closest point of the estimated vessels. Because the assumption of normality of the collected distances distribution is not verified, we analyze this distribution using boxplots [21]. These plots display the maximum and minimum values, as well as a central box indicating the location of the 50% central values between the lower and upper quartile. Outliers are also detected and displayed on these plots. Fig. 4 presents the boxplots of the distances distribution for  $\sigma_{\text{noise}}$  varying from 5 to 25. Our algorithm seems to be quite accurate: for a noise variance below 15, all the distances, except outliers, equal zero; for higher noise variance, the distribution interquartile range is always inferior to 0.7 mm and the min. and max. values are  $-1$  and  $\sqrt{3}$  mm, respectively. As previously discussed, the radius overestimation phenomenon is also observed on the boxplots as the interquartile range is spread between 0 and a positive value. Fig. 5 compares the accuracy of the three methods in presence of noise ( $\sigma_{\text{noise}}$  of 20 in this case). The region-growing method is clearly unsuitable at this level of noise. The classical graph cuts and our methods show boxplots with almost a similar range. However, our method has a smaller interquartile range, min and max a bit closer and less

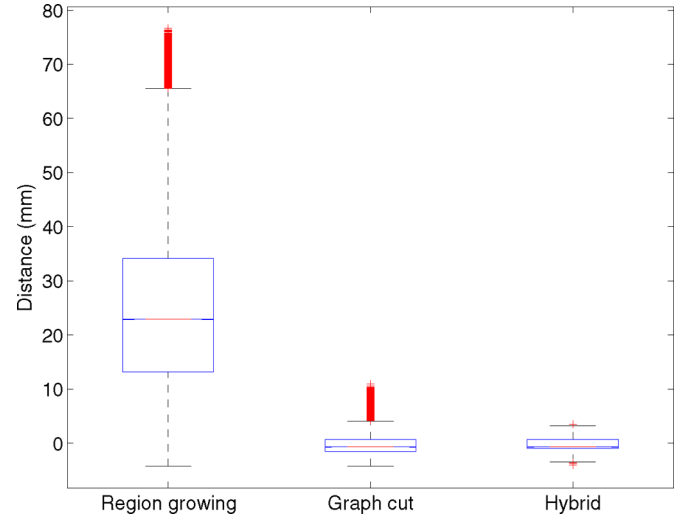


Fig. 5. Distance to the border boxplots for the three different methods with a variance of 20.

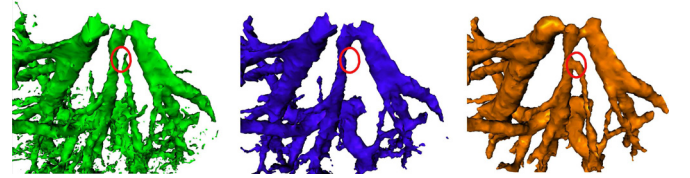


Fig. 6. Comparison of the three segmentation methods. (a) Region-growing. (b) Graph cuts. (c) Hybrid method. Red circles highlight the ability of the different methods to extract and connect a specific vascular branch.

outliers. That is to say that the introduction of the cylindrical model enhance the accuracy of the segmentation.

### B. Segmentation Results on Real Data

This algorithm has been tested on clinical abdominal CT volumes acquired during four different contrast medium diffusion phases: before injection, arterial, portal, and delayed phases. Each of the volumes has the following properties: approximately  $120 \times 512 \times 512$  pixels slices with a slice resolution of 0.7 mm and an interslice spacing of 2 mm. The parameters set for the method in the presented result is (see Table I):  $\lambda_1 = 0.3$ ,  $\lambda_2 = 0.1$ ,  $\lambda_3 = 0.6$ , and  $\sigma = 0.14$  with a 26-neighborhood connectivity. A bounding box region of interest is interactively defined in order to minimize the memory impact of the graph.

First, we compare the ability of the three previously mentioned methods to segment the vascular trees on real data (the portal phase volume in this case). In Fig. 6, we can notice that the region growing is biased by the noise induced by the microvascularization. The classical graph cuts is less sensitive to this noise. However, some branches are not detected (e.g., under the red circle). This figure highlight the ability of our method to better extract and connect branches in a real situation, thus, without any manual interaction.

We will now show some segmentation results obtained on two different diffusion phases' volumes acquired during a

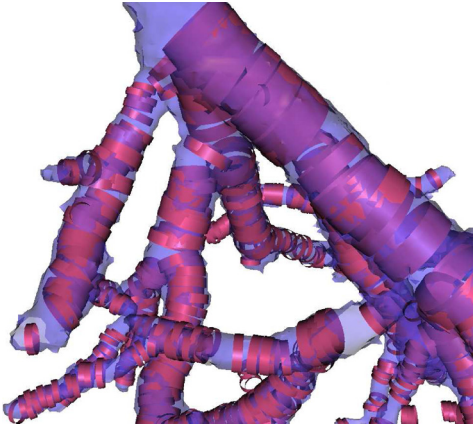


Fig. 7. Visualization of the extracted vascular structures superimposed on the detected cylinders seen by transparency.

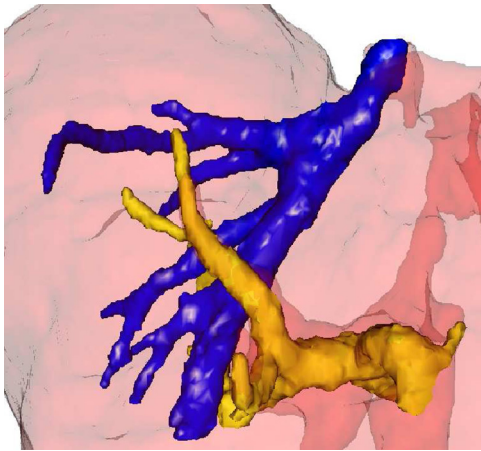


Fig. 8. Visualization of the portal (dark blue) and hepatic (yellow) venous trees.

patient study. We applied our method on the portal phase volume (see Figs. 7–9) that presents the highest vascular contrast enhancement for the venous trees and also on the arterial phase volume (see Fig. 10). Due to the fact that we did not perform a registration between these two volumes, the segmentation results will be shown separately.

The use of the local geometrical model to constrain the graph cuts can be directly seen on Fig. 7. In this figure, we superposed the final extracted vascular structure on the local cylinder models estimated by our geometrical moments-based detector. We can observe the good correlation in diameter, position, and orientation between the identified models and the final extracted vessel. We can also see that the estimated local models constrain the graph cuts process in a correct manner.

The exhaustive application of the process on the complete volume data allows us to extract, automatically and simultaneously, the main branches of both the portal (in dark blue) and hepatic (in light yellow) venous vascular trees (see Fig. 8). Even if the two trees were simultaneously extracted, they were not connected to one another. It was so easy to label them manually.

The method is accurate enough to characterize the tumor-neighboring vascularization (see Fig. 9). In this figure, the tumor

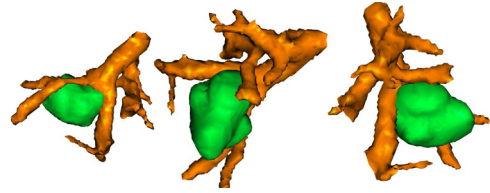


Fig. 9. Visualization of the tumor and its neighboring vascularization.

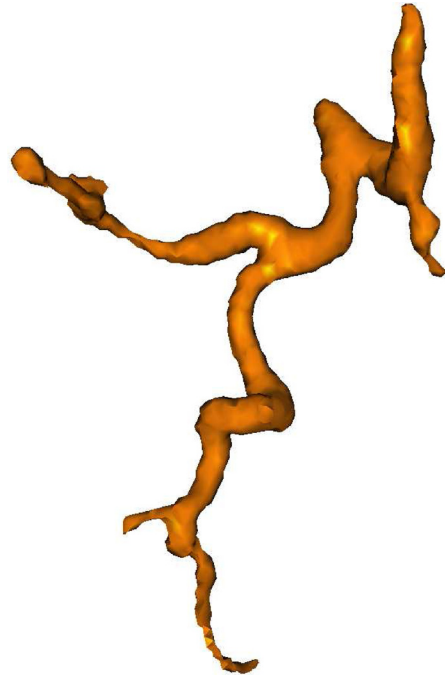


Fig. 10. Visualization of the hepatic arterial tree.

has been separately characterized using the classical graph cuts method [6]. We then applied the hybrid method in the region of interest around the tumor. In this region, we adapted the intensities *a priori* in order to recover thinner vascular branches. Such results are directly related to our medical problems and can serve as the anatomical description for a patient-specific dosimetry modeling and planning.

In Fig. 10, the hepatic artery was extracted when we applied our algorithm on the early acquisition phase study. In our actual stage of research, the venous trees and the arterial tree were extracted and displayed separately, but a nonrigid registration scheme permitting them to mix together, allowing a fully integrated description of the hepatic vascularization.

The overall computation process (detection and graph cuts segmentation) takes between 10 and 100 s on a 1.6 GHz Xeon, 4 Go RAM PC, according to the size of the candidate voxels map.

### C. Discussion

The moment-based detector gives consistent local information about the vessel diameter. The integration of this information, as a constraint in the graph cuts algorithm, allows extracting the hepatic vessel trees. An extensive validation on synthetic

data has shown the superiority of our algorithm compared to the classical graph cut, both in term of robustness and accuracy. The dice measure and overall distance between the phantom and the segmented data are relevant. Moreover, it has been shown that if the goal of the segmentation is the detection of all the branches versus radius accuracy, we can enhance the  $\lambda_3$  value, and hence, enabling the extraction in extreme noisy condition.

The final result on real dataset shows accurate vessel-diameter estimation and good tree tracking that takes the bifurcations into account. As previously expected, our method allows us to overcome the shrinking bias on elongated structures, which is the weak point of the graph cuts method, while simultaneously correctly handling the bifurcations by reconnecting the vascular subtrees, problematic in geometrical tracking. Our objective to describe the tumor's neighboring vascularization is also achieved.

However, some drawbacks remain. The drawbacks are primarily caused by the fact that the local model detection/estimation scheme is exhaustively applied on the whole volume, in opposition to a geometrical tracking, which are as follows.

- 1) The diameter estimation is computed from intensities *a priori*. In our case, these *a priori* are global. When the tissues are very heterogeneous, this intrinsic limitation can lead to a diameter misestimation or, in the worst case scenario, the thinnest part of the vessel not being detected. This problem can be solved by an adaptive estimation of the intensities *a priori*.
- 2) Background noise can induce some false detections. Thus, filters such as 3-D anisotropic diffusion or 3-D Gaussian can be applied on the volume before the segmentation process.
- 3) This method gives better results when applied on an anisotropic dataset. Indeed, when an interpolation is applied in order to recover isotropy, some noise can be elongated along the interpolation direction, and then, be estimated as cylinder-like structures, resulting in false detections.

In conclusion, this method presents promising results. It is sufficiently generic to segment any vascular tree when the few parameters (intensities *a priori*, minimum and maximum vessel radius size) are correctly adjusted. The computation times are compatible with a clinical context attributes.

#### IV. CONCLUSION

A fast and fully automatic method for the segmentation of the hepatic vessel trees has been presented. It is based on a graph cuts technique constrained by local vessel models in order to take advantage of both approaches: accuracy and robustness of the local modeling and global optimality of the graph cuts technique. We validate our method on synthetic data, and then, applied it on several CT databases acquired on different contrast medium diffusion phases. The obtained results proved that our approach is robust and fast enough to be used in a clinical context. Moreover, this method allowed us to describe the patient-specific vascularization surrounding a HCC. Such infor-

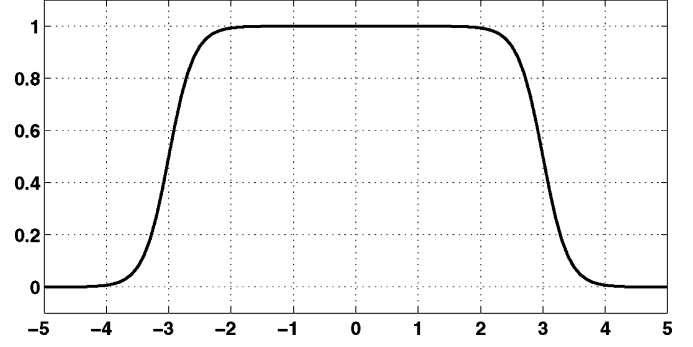


Fig. 11. Example of  $f_{\text{axis}}(r)$  for radius  $R_i = 3$  and a sigmoid slope  $K = 5$ . Abscissa index 0 corresponds to the vessel center.

mation is of crucial importance for the definition of accurate and patient-adapted hyperthermia therapy planning.

#### APPENDIX

##### Diffusion map of the cylinder information

Given a cylinder with index  $i$  of radius  $R_i$  in a center-oriented coordinates system  $x, y$ , and  $z$  with  $z$  the cylinder axis, the local diffusion map  $\text{DiffMap}_i$  is created by the product of two diffusion functions as follows:

$$\text{DiffMap}_i(x, y, z) = f_{\text{axis}}(x, y, z) f_{\text{radius}}(x, y, z) \quad (4)$$

with the following.

- 1)  $f_{\text{axis}}$  being a function promoting the diffusion along the cylinder axis. We choose a Gaussian with  $\sigma$  set to  $2R_i$  as follows:

$$f_{\text{axis}}(x, y, z) = \frac{1}{2R_i \sqrt{2\pi}} \exp\left(-\frac{z^2}{8R_i^2}\right). \quad (5)$$

- 2)  $f_{\text{radius}}$  being a function constraining the diffusion perpendicularly to the cylinder axis. Perpendicular to the axis, the vessel shape is described by the difference of two sigmoid functions (see Fig. 11). The parameters of this function are:  $R_i$  the vessel radius and a slope  $K$ . If  $r$  is the perpendicular distance from a point  $p(x, y, z)$  to the cylinder axis ( $r = \sqrt{x^2 + y^2}$ ), then

$$f_{\text{radius}}(x, y, z) = \frac{1}{1 + \exp^{-K(r+R_i)}} - \frac{1}{1 + \exp^{-K(r-R_i)}}. \quad (6)$$

The final costs map  $C_{\text{vessel}}$  is the result of the mixture of the local maps after translation and rotation, according to the cylinders orientation as follows:

$$C_{\text{vessel}} = \sum_{i=1}^N \text{DiffMap}_i \quad (7)$$

with  $N$  the number of extracted cylinders.

#### REFERENCES

- [1] H. B. El-Serag and A. C. Mason, "Rising incidence of hepatocellular carcinoma in the United States," *N. Engl. J. Med.*, vol. 340, no. 10, pp. 745–750, 1999.



- [2] R. A. Lencioni, H. P. Allgaier, D. Cioni, M. Olschewski, P. Deibert, L. Crocetti, H. Frings, J. Laubenberger, I. Zuber, H. E. Blum, and C. Bartolozzi, "Small hepatocellular carcinoma in cirrhosis: Randomized comparison of radio-frequency thermal ablation versus percutaneous ethanol injection," *Radiology*, vol. 228, no. 1, pp. 235–240, 2003.
- [3] C. Lafon, J. Y. Chapelon, F. Prat, F. Gorry, J. Margonari, Y. Theillere, and D. Cathignol, "Design and preliminary results of an ultrasound applicator for interstitial thermal coagulation," *Ultrasound Med. Biol.*, vol. 24, no. 1, pp. 113–122, 1998.
- [4] B. Seket, C. Lafon, F. Mithieux, C. Goldenstedt, C. Paquet, J. Y. Chapelon, J. Y. Scoazec, M. Rivoire, and D. Cathignol, "Developing an interstitial ultrasound applicator for thermal ablation in liver: Results of animal experiments," *J. Surg. Res.*, vol. 142, no. 1, pp. 81–89, 2007.
- [5] B. van Ginneken, T. Heimann, and M. Styner, "3-D segmentation in the clinic: A grand challenge," in *Proc. Workshop 3-D Segmentation Clinic—A Grand Challenge—MICCAI 2007*, Brisbane, pp. 7–15.
- [6] S. Esneault, N. Hraich, E. Delabrousse, and J.-L. Dillenseger, "Graph cut liver segmentation for interstitial ultrasound therapy," in *Proc. 29th Conf. IEEE Eng. Med. Biol. Soc.*, Lyon, 2007, pp. 5247–5250.
- [7] C. Kirbas and F. Quek, "A review of vessel extraction techniques and algorithms," *ACM Comput. Surv.*, vol. 36, no. 2, pp. 81–121, 2004.
- [8] D. Selle, B. Preim, A. Schenk, and H. Peitgen, "Analysis of vasculature for liver surgical planning," *IEEE Trans. Med. Imag.*, vol. 21, no. 11, pp. 1344–1357, Nov. 2002.
- [9] L. M. Lorigo, O. D. Faugeras, W. E. L. Grimson, R. Keriven, R. Kikinis, A. Nabavi, and C.-F. Westin, "Curves: Curve evolution for vessel segmentation," *Med. Image Anal.*, vol. 5, pp. 195–206, 2001.
- [10] K. Krissian, G. Malandain, N. Ayache, R. Vaillant, and Y. Troussset, "Model based detection of tubular structures in 3-D images," *Comput. Vis. Image Understanding*, vol. 80, no. 2, pp. 130–171, 2000.
- [11] P. Reuzé, J.-L. Coatrieux, L. Luo, and J.-L. Dillenseger, "A 3-D moment based approach for blood vessel detection and quantification in MRA," *Technol. Health Care*, vol. 1, no. 2, pp. 181–188, 1993.
- [12] C. Toumoulin, C. Boldak, J.-L. Dillenseger, J.-L. Coatrieux, and Y. Roland, "Fast detection and characterization of vessels in very large 3-D data sets using geometrical moments," *IEEE Trans. Biomed. Eng.*, vol. 48, no. 5, pp. 604–606, May 2001.
- [13] L. Luo, C. Hamitouche, J.-L. Dillenseger, and J.-L. Coatrieux, "A moment-based three-dimensional edge operator," *IEEE Trans. Biomed. Eng.*, vol. 47, no. 7, pp. 693–703, Jul. 1993.
- [14] D. M. Greig, B. T. Porteous, and A. H. Scheult, "Exact maximum a posteriori estimation for binary images," *J. R. Stat. Soc. B*, vol. 51, no. 2, pp. 271–279, 1989.
- [15] Y. Boykov, O. Veksler, and R. Zabih, "Fast approximate energy minimization via graph cuts," *IEEE Trans. Pattern Anal. Mach. Intell.*, vol. 23, no. 11, pp. 1222–1239, Nov. 2001.
- [16] Y. Boykov and M.-P. Jolly, "Interactive graph cuts for optimal boundary & region segmentation of objects in N-D images," in *Proc. 8th Int. Conf. Comput. Vis. (ICCV 2001)*, Vancouver, vol. 1, pp. 105–112.
- [17] Y. Boykov and G. Funka-Lea, "Graph-cuts and efficient N-D image segmentation," *Int. J. Comput. Vis.*, vol. 70, no. 2, pp. 109–131, 2006.
- [18] L. Ford and D. Fulkerson, "Maximal flow through a network," *Can. J. Math.*, vol. 8, pp. 399–404, 1956.
- [19] Y. Boykov and V. Kolmogorov, "An experimental comparison of min-cut/max-flow algorithms for energy minimization in vision," *IEEE Trans. Pattern Anal. Mach. Intell.*, vol. 26, no. 9, pp. 1124–1137, Sep. 2004.
- [20] G. Yang, A. Bousse, C. Toumoulin, and H. Shu, "A multiscale tracking algorithm for the coronary extraction in MSCT angiography," in *Proc. 28th Conf. IEEE Eng. Med. Biol. Soc.*, New York, 2006, pp. 3066–3069.
- [21] D. Hoaglin, F. Mosteller, and J. Tukey, *Understanding Robust and Exploratory Data Analysis*. New York: Wiley, 1983.



**Simon Esneault** was born in Angers, France, in 1982. He received the engineer degree in telecommunication and networking from the École Nouvelle d'Ingénieurs en Communication Telecom Engineering School, Lille, France, and the M.S. degree in signal and image processing from the University of Rennes 1, Rennes, France. He is currently working toward the Ph.D. degree with the Laboratoire de Traitement de l'Image et du Signal, Institut National de la Santé et de la Recherche Médicale, Université de Rennes 1.

His current research interests include high-intensity focused ultrasound liver therapy planning for primary tumors, including CT image segmentation, and modeling of the effect induced by the therapy.



**Cyril Lafon** (M'03) was born in Saint Yrieix la Perche, France, in 1974. He received the B.Sc. degree in physics from Blaise Pascal University, Clermont-Ferrand, France and University of Montreal, QC, in 1995, and the Ph.D. degree in biomedical engineering from the University Claude Bernard Lyon 1, Lyon, France, in 1999.

He was a Postdoctoral Research Fellow with the Applied Physics Laboratory, University of Washington, Seattle, where he was involved in ultrasound-induced hemostasis and the development of tissue mimicking phantoms for high-intensity focused ultrasound applications. Since 2002, he has been a Research Scientist with Institut National de la Santé et de la Recherche Médicale, Université Claude Bernard Lyon 1. His current research interests include modeling ultrasound wave propagation, development of ultrasonic therapeutic devices for thermal ablation or drug delivery, and communication by ultrasound for medical applications.



**Jean-Louis Dillenseger** received the electrical engineering degree from the National Engineer School of Brest, Brest, France, in 1988, and the Ph.D. degree in biomedical engineering from the University of Tours, Tours, France, in 1992.

He is currently an Associate Professor with the Laboratoire Traitement du Signal et de l'Image, INSERM U642, University of Rennes 1, Rennes, France. His research interests include image processing, image-guided surgery, and scientific visualization applied in biomedical areas.